Journal of Materials Chemistry B

Nanoscale 3D printing of hydrogels for cellular tissue engineering

Journal:	*Journal of Materials Chemistry B*
Manuscript ID	TB-REV-02-2018-000301.R1
Article Type:	Review Article
Date Submitted by the Author:	07-Mar-2018
Complete List of Authors:	You, Shangting; University of California San Diego, Nanoengineering Li, Jiawen; Univerisity of science and technology of China, Department of Precision Machinery and Precision Instrumentation Zhu, Wei; University of California San Diego, NanoEngineering Yu, Claire; University of California San Diego, Nanoengineering Mei, Deqing; Zhejiang University, College of Mechanical Engineering Chen, Shaochen; University of California San Diego, Nanoengineering

Nanoscale 3D printing of hydrogels for cellular tissue engineering

Shangting You[1*], Jiawen Li[1,2*], Wei Zhu[1], Claire Yu[1], Deqing Mei[3], Shaochen Chen[1]

1. Department of NanoEngineering, University of California, San Diego, La Jolla, CA 92093–0448, USA
2. Department of Precision Machinery and Precision Instrumentation, University of Science and Technology of China, Hefei, 230026, China
3. Department of Mechanical Engineering, Zhejiang University, Hangzhou, 310027, China

*You and Li contributed equally in this work; Corresponding author: chen168@eng.ucsd.edu

Abstract

Hydrogel scaffolds that mimic the native extracellular matrix (ECM) environment is a crucial part of tissue engineering. It has been demonstrated that cell behaviors can be affected by not only the hydrogel's physical and chemical properties, but also its three dimensional (3D) geometrical structures. In order to study the influence of 3D geometrical cues on cell behaviors as well as the maturation and function of engineered tissues, it is imperative to develop 3D fabrication techniques to create micro and nanoscale hydrogel constructs. Among existing techniques that can effectively pattern hydrogels, two-photon polymerization (2PP)-based femtosecond laser 3D printing technology allows one to produce hydrogel structures with 100 nm resolution. This article reviews the basics of this technique as well as some of its applications in tissue engineering.

1. Introduction

Hydrogels are three-dimensionally cross-linked hydrophilic polymer chains systems [1] which have high water content comparable to that of soft tissues [2]. Due to the vast properties of hydrogels such as tunable mechanical and chemical properties, biocompatibility, capability to act as a cellular growth medium, and ability to mimic the extracellular matrix (ECM), they have been widely investigated in various biomedical applications, including tissue engineering scaffolds [3–5], organ-on-a-chip [6], controlled release drug delivery systems [7], and biosensors [8,9]. The 3D shape and size of hydrogels have been proven to be of vital importance in a myriad of studies [10]. For example, alginate hydrogel spheres with a smaller diameter (300–500 μm) transplanted into the mice elicited a severe fibrotic response, whereas those with a larger size (1.5–1.9 mm) did not elicit any severe fibrotic response [11]. Also, circular rods produced lower extent of foreign body response, compared to pentagonal and triangular geometries [12]. Microscale hydrogels, namely microgels, with specific 3D shapes have been used to mimic the functional units of different tissues [13], which can be further assembled to fabricate large cellular constructs [14]. Furthermore, disc-shaped microgels for drug delivery have been reported to have a higher targeting efficiency than those with spherical geometry [15]. As a result, the advancement of current manufacturing techniques for the fabrication of 3D hydrogel constructs with controllable geometry and dimensions can have profound impact in the biomedical engineering field.

Numerous strategies have been developed and utilized to fabricate complex 3D hydrogel constructs, including molding [16,17], soft lithography [18], and extrusion-based 3D printing [19]. However, there are limitations associated with these existing methods [20]. For instance, the molding method requires the redesign and preparation of a second mold for a different geometry, while soft lithography and nanoimprinting are intrinsically two-dimensional (2D) fabrication methods.

Extrusion-based 3D printing is capable of fabricating 3D structures with flexible geometrical control, but the fabrication resolution falls in the range of tens to hundreds of microns, which is limited in accurately mimicking the natural biological cues in micron or submicron scale [21].

With the rapid advancement of the tissue engineering field, an alternative fabrication method that is capable of fabricating 3D structures with submicron resolution and precise control of the geometry is highly desired. Femtosecond laser induced two-photon polymerization (2PP) is a promising 3D printing technique which has been applied to many fields such as nanophotonics [22], micro-electromechanical systems [23], microfluidics [24], biomedical implants and microdevices [25]. 2PP can print designed and ultraprecise 3D structures with high spatial resolution in nanoscale. It is a powerful fabrication method for creating 3D hydrogels with precise control of the size and shape for tissue engineering and drug delivery applications.

In this article, we review the recent advances of nanoscale 3D printing of hydrogels by 2PP and its applications in tissue engineering and cell biology. We first introduce the basic principles of 2PP, the typical system setups, and the material library for 2PP in Section 2. In Section 3, we emphasize on some specific photoinitiators and hydrogel materials as well as their applications in cellular and tissue engineering. In Section 4, we will discuss and highlight the future perspectives of this printing technique.

2. Two-photon polymerization

2PP has been demonstrated as a promising technology for the fabrication of 3D structures with high resolution. When an ultrafast infrared laser beam is tightly focused into the volume of a photosensitive material, the polymerization process can be initiated by two-photon absorption (2PA) within the focal region. By moving the laser focus three-dimensionally through the photosensitive material arbitrary 3D structures can be fabricated [26].

2.1 2PP principles

The foundation of 2PP is 2PA. 2PA is defined as the simultaneous absorption of two photons of identical or different frequencies in order to excite a molecule from one state to a higher energy level. The energy difference between these states is equal to the sum of the energies of the two photons. The concept of 2PA was first conceived by Goeppert-Mayer in 1931 and demonstrated in an experiment by Kaiser in 1961 after the invention of the laser, which enabled the generation of two-photon excited fluorescence in an europium-doped crystal [27].

Following the invention of ultrafast lasers, researchers have expanded the application of 2PA into the micro/nano-fabrication field using 2PP [28]. As shown in Fig. 1(a), the photoinitiator absorbs two photons simultaneously to reach S1 state, then transits to T1 state by inter-system crossing, and finally transits back to the ground state and releases a free radical (R*). The free radicals then initiate chain reaction polymerization of the monomers to form solid state long-chain polymers.

2PA requires an extremely high power density at the focal point for the reaction. The peak power of a femtosecond laser is much higher than a continuous wave laser or a nanosecond pulsed laser owing to the femtosecond laser pulse width that results in extremely high photon density in the focal region, which meets the power density requirement of 2PA. One major advantage of 2PP over traditional single photon polymerization (1PP) is the 3D fabrication capability inside the hydrogel. A femtosecond laser emits infrared or near-infrared light, which cannot initiate the single photon polymerization [29]. On the other hand, 2PP can only be initiated within the focal region. Therefore, a femtosecond laser beam is able to penetrate a photoresist and induce polymerization inside the liquid at the focal point without polymerizing the material along its path. Fig. 1(b) and Fig. 1(c) show the difference between 2PP and 1PP. 2PP causes polymerization only at the focal point of the laser beam, resulting in a thin helical line along the trace of the moving

laser focus, while 1PP causes polymerization in the whole light path resulting in thick helical walls. Due to the energy threshold requirement of 2PP , nanoscale resolution can be achieved by controlling the laser-pulse energy and writing speed [30–32].

2.2 Equipment and experimental setup

A typical 2PP experimental system and procedure for fabricating a 3D structure is shown in Fig. 2. The system includes: (1) an ultrafast pulsed laser, (2) a scanning system, (3) beam focusing optics, (4) a beam intensity control and a beam shutter, and (5) a computer with control software. The laser beam is tightly focused into the volume of the material and moves along the designed path where the material is polymerized and solidified [27].

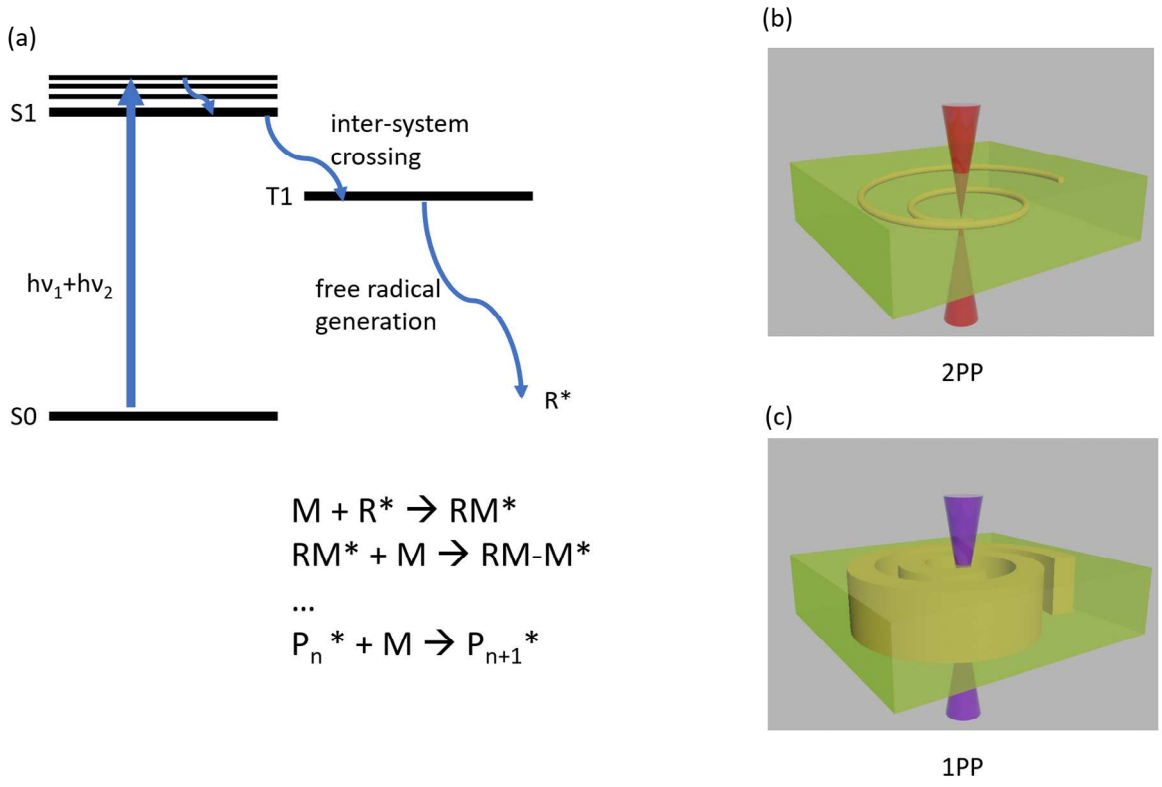

Fig.1 (a) Jablonski diagram and chain reaction polymerization process of 2PP. (b) Schematic diagram of 2PP fabrication. (c) Schematic diagram of 1PP fabrication. M: monomer. R*: free radical. P_n: polymer consists of n monomer units.

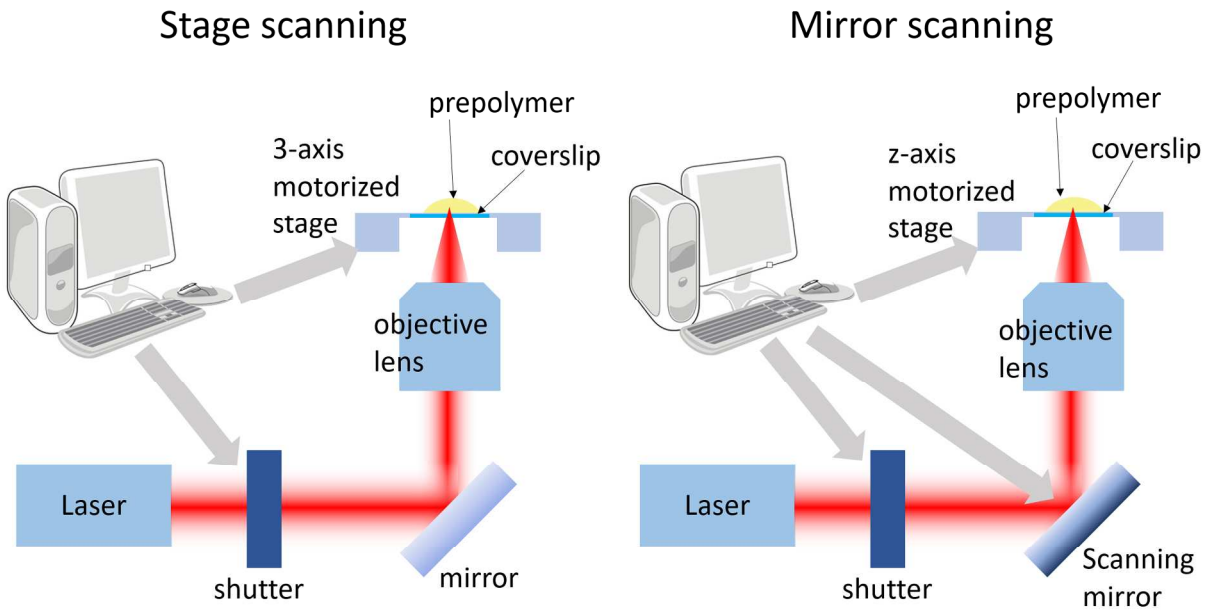

Fig. 2 Typical setup of a 2PP fabrication system. Left: stage scanning type setup, where the stage scans in x, y, and z directions. Right: mirror scanning type setup, where the stage scans in z direction, and the scanning mirror scans in x and y directions.

A typical laser source for 2PP is the mode-locked Ti:Sapphire femtosecond laser operating at around 800 nm. Recently, second-harmonic fiber lasers that typically operate at 780 nm have gained popularity because they are more reliable and affordable. The energy required for the polymerization process depends on the monomer, the photoinitiator and the objective lens. Typical 2PP laser sources produce pulses with a duration of tens to hundreds of femtoseconds at a repetition rate of around 80 MHz, and the energy is usually in the order of a few nanojoules per pulse.

In order to 'write' the 3D structure into the photosensitive polymer, nanofabrication by 2PP can be performed by moving either the beam focus, or the monomer solution. In the first case, a set of galvanometric scanning mirrors are used to scan the excitation beam in the x and y directions and a

piezo stage is used to move the monomer solution or the objective lens up and down. In the second scheme, the monomer solution is moved in all three directions with the aid of a three-axis stage. Although both techniques have proven to be effective in the fabrication of 3D nanostructures, they have complementary advantages that should be considered when choosing one system over the other. When using stage scanning setup for structure writing, it has a large scanning range but relatively slow scanning speed than the mirror scanning setup. Scanning mirror has the advantage of higher scanning speeds (up to m/s) than a stage. However, as the beam moves, the pattern area can be distorted because the objective lens, even if it is planar, does not provide a completely flat field-of-view. For this reason, scanning mirrors are not used for applications where high accuracy is needed (e.g. photonic device applications). On the other hand, they are very commonly used in bioengineering applications in which nanometer accuracy is not essential. Another disadvantage of the mirror scanning method is that the scanning range is within the field of view of the objective, which is very small. In practice, most systems have both galvanometric scanners and high-accuracy xyz stages and switch between the two scanning modes according to the application requirements. Notably, both setups are capable of having high reproducibility.

The need for a high laser intensity for multi-photon absorption and the expectation of a high fabrication resolution can be achieved by a tightly focused laser beam, which requires a high numeric aperture (NA) microscope objective lens. One disadvantage of using a microscope objective is the short working distance, which limits the height of the fabricated structures. To address this issue, the "dip-in" lithography [33] and the widened objective working range two-photon polymerization (WOW-2PP) technology [34] were developed, where the microscope objective was immersed into the liquid photopolymer for the fabrication.

In addition, the beam intensity can be controlled using neutral density filters or a combination of a

polarizer and a waveplate. A fast mechanical shutter or an acousto-optic modulator can be used to control the on/off state of the beam. A computer with control software is used to control and synchronize the optical and mechanical components described above.

2.3 Material system for 2PP

In general, a material suitable for photopolymerization includes at least two components: (i) a monomer or a mixture of monomers/oligomers, which will crosslink and form the final polymer and (ii) a photoinitiator, which will absorb the laser photons and provide free radicals that will induce the polymerization [27]. Both the photoinitiator and the monomer/oligomer are transparent at the laser wavelength used, such that the laser beam can be focused inside the volume of the material without being absorbed at the surface. Several photoinitiator and monomer/oligomer combinations have been previously used for 2PP [35].

During polymerization, a monomer is converted into polymer and this transformation can be induced by light. In 1PP, a photoinitiator absorbs the light and produces an active species which induces the photopolymerization. However, 2PP is more complicated and extra requirements must be met for the polymerization to occur [33,36]. Namely, the photoinitiator needs to have a high two-photon absorption cross-section and a high radical quantum yield, therefore only a few photoinitiators compatible with 1PP can be used for 2PP [37].

An effective 2PP photoinitiator has a high quantum yield in the generation of active moieties, thermally stable at fabrication temperature (e.g. room temperature), optically stable in the dark, and soluble in the polymerization medium [38]. Photoinitiators generate free radicals, which initiate the polymerization process of acrylates or vinyl ethers [39,40]. The most commonly used free radical photoinitiators are benzophenone and its derivatives [26]. Recently, there have been a lot of efforts in synthesizing fast and efficient photoinitiators specifically for multi-photon applications [41].

In addition to monomers and photoinitiators, the material system for 2PP may also contain solvent and other additive. For instance, nanoparticles can be incorporated into the material system to obtain desired mechanical [42] and electrical [43] properties.

3. Nanoscale 3D printing of hydrogel materials

In human tissues, cells receive numerous signals from their natural extracellular matrix (ECM) surroundings, which has significant influence on the cellular behaviors [44.] Researchers have focused on mimicking key characteristics of the ECM to study cell responses to different mechanical, chemical, and topographical cues. Hydrogels are attractive materials for various biomedical applications because they are structurally similar to the ECM. A wide range of synthetic and naturally derived materials can be used to form hydrogels for tissue engineering [45].

3.1 Water Soluble, Two-Photon Active Photoinitiators

A two-photon photoinitiator is a photoactive molecule, which simultaneously absorbs two photons upon nonlinear excitation to directly or indirectly induce the generation of free radicals for subsequent polymerization [46]. In principle, the photoinitiator molecule should possess a high initiation efficiency, good biocompatibility, acceptable hydrophilicity, and low cytotoxicity. Highly active photoinitiators are critical for efficient 2PP which is characterized by a high 2PA cross section (σ_{2PA}) and high initiating efficiency leading to a broad processing window and low polymerization threshold. Polymerization performed at low excitation power and short exposure time leads to high polymerization speeds and high quality structures [47]. From the biomedical application perspective, in addition to the desired high yield of radical generation, these photoinitiators should not affect the biological environment. The ideal structures should be highly hydrophilic and noncytotoxic, and these aspects should be considered while choosing the 2PP

photoinitiators.

Chichkov *et al.* successfully fabricated biocompatible scaffolds using commercially available inorganic-organic hybrid formulations with the UV initiator Irgacure 369 as photoinitiator [48,49]. Although the 2PA cross section of Irgacure 369 is small at the desired wavelength, the limited 2PA could be compensated by high radical formation quantum yields to ensure acceptable initiation efficiency [37].

To form hydrogels via 2PP, researchers first used commercial hydrophobic UV photoinitiators to fabricate hydrophilic constructs from water soluble monomers [50,51]. Using this approach, cells cannot be incorporated into the fabrication process due to the lack of aqueous suspension environment. One strategy to improve water solubility of commercially available, hydrophobic initiators is to make use of nonionic surfactants. Jhaveri *et al.* increased the water solubility of commercial hydrophobic initiators (Irgacure 651 and AF240) using a nonionic surfactant (Pluronic F127). Although this approach enables the fabrication of hydrogel structures from an aqueous formulation, a large amount of surfactant is needed to ensure adequate initiation efficiency, which might reduce the biocompatibility. Therefore, there remains a need for the development of real water soluble initiating systems for 2PP [52].

Irgacure 2959 was used for 2PP of 3D scaffolds due to its hydrophilicity and good biocompatibility. Ovsianikov *et al.* used Irgacure 2959 to form a support for the culture of human adipose-derived stem cells [53]. This photoinitiator was chosen because of its reasonable hydrophilicity and reduced cytotoxicity. Also, the hydroxyl group enhances the compatibility of Irgacure 2959 in water-borne coating formulations. The final hydrogel structures not only preserved the enzymatic degradation of gelatin after the 2PP process, but also supported cell proliferation at normal rate.

Lithium phenyl-2,4,6-trimethylbenzoylphosphinate (LAP) is another biocompatible water-soluble

photoinitiator. Zhang *et al.* used LAP to fabricate suspending hydrogel networks that exhibit tunable Poisson's ratio and investigated the 10T1/2 cellular response. [54]

The most popular hydrophilic initiation system for 2PP is a dye-amine combination. With the desired absorption above 400 nm and easy accessibility, commercially available hydrophilic xanthene dyes, such as rose bengal, eosin Y, and erythrosine were applied in 2PP with amine as co-initiator [55]. Some hydrophilic dyes, such as rose bengal [56] and methylene blue [57,58], could also be used to directly crosslink proteins.

The most effective way to produce efficient water soluble 2PA photoinitiators is to introduce water-borne functional groups, such as quaternary ammonium cations or different carboxylic sodium salts into the known core structures of the chromophore possessing high 2PA activity [25]. Suitable spacers like alkyl-chains are usually required to avoid shifting the electronic structure of the 2PA chromophore. A distyrylbenzene chromophore (WSPI) with quaternary ammonium cations was initially synthesized to study the solvent effects on the 2PA behavior. Using WSPI as an efficient initiator, Torgersen *et al.* fabricated 3D hydrogel scaffolds in the presence of a living organism for the first time [59]. Their recent research on a series of hydrophobic benzylideneketone dyes shows that different sizes of the central rings have significant effects on their activity as initiators for 2PP [38]. The 4-methylcyclohexanone based initiator G2CK showed broader processing windows than its counterparts and the reference molecule WSPI. Complex structures could be fabricated at high fabrication speed using 50% poly(ethylene glycol) diacrylate (PEGDA) based formulations dissolved in aqueous solution. Moreover, the cytotoxicity of G2CK is as low as Irgacure 2959 when exposing human osteosarcoma MG63 cell lines to the molecules in cell culture media. In a similar manner, Ovsianikov *et al.* used the benzylidenecycloketones (G2CK and P2CK) as photoinitiators to fabricate well-defined microstructures [60]. Xing *et al*. fabricated 3D

hydrogel structure with WI, which is a water soluble 2PP photoinitiator prepared by host-guest chemical interaction. [61]

3.2 Hydrogels precursors

Although a highly efficient water soluble two-photon photoinitiator is the prerequisite for 2PP of hydrogels, the use of appropriate photopolymerizable monomers/macromers as hydrogel precursors is equally important. From the biological point of view, the hydrogel precursors should possess sufficient water solubility and must be cytocompatible.

A hydrogel is a 3D network of hydrophilic polymer chains that are crosslinked through either physical bonding or chemical bonding, in the presence of water. In essence, hydrogels are water-swollen gels with polymeric structures holding together. Over the past 20 years, a variety of natural and synthetic polymers have been utilized to prepare hydrogels [62]. There are a number of ways to categorize hydrogels [63], based on preparation methods, ionic charge or physic-chemical structural features. The majority of hydrogel biomaterials typically fall into one of three major categories: (i) natural polymers and proteins, (ii) synthetic hydrogels, and (iii) modified natural hydrogels.

Natural hydrogels using biological polymers as building blocks have been widely used because of their inherent excellent biocompatibility, low toxicity, and susceptibility to enzymatic degradation. Examples of naturally derived hydrogels include collagen, hyaluronic acid (HA), alginate, and fibrin. Natural hydrogels are more efficient at mimicking the biological nature of the native extracellular matrix [62].

Most recently, synthetic hydrogels have gained popularity for tissue engineering applications owing to their improved material properties (i.e. mechanical strength) and reduced handling difficulty in comparison to their natural counterparts. Synthetic hydrogels are completely

synthesized in the laboratory. The most popular synthetic hydrogel is polyethylene glycol (PEG). It is FDA (Food and Drug Administration)-approved for many biomedical uses and can exist in a lot of different formulations, which have been extensively used in 2D and 3D printing for medical devices [64,65]. PEGDA, as well as polyacrylamide (PAAM)-based gels are common examples of synthetic hydrogels for photopolymerization. In general, synthetic materials allow for more fine-tuned control over chain length and distributions, as well as crosslinking densities, allowing for precise modulation of specific mechanical properties.

Modified natural hydrogels are typically natural hydrogels that are chemically modified with some functional groups in lab. This kind of hydrogels maintain good biocompatibility of natural hydrogels, and in the meanwhile they have some favorable material properties such as photopolymerizability, tunable mechanical strength, etc. A widely used modified natural hydrogel is gelatin methacrylate [66,67].

3.2.1 Natural hydrogel precursors for two photon cross-linking

The multiphoton polymerization of natural polymers and proteins has been pioneered by Campagnola and his co-workers, who worked with a variety of cross-linked proteins such as bovine serum albumin (BSA), fibrogen, fibronectin, and collagen [68]. Campagnola *et al.* used 2PP and naturally biocompatible macromolecules to create simple multidimensional structures from BSA or fibrinogen. The hydrogel cross-linking process involved transferring a hydrogen from the protein to the photoexcited photoinitiator Rose Bengal. The process likely occurs at the ketone of the Rose Bengal because the triplet state ketones abstract the protons and are reduced to alcohols, leading to the inability of the photoinitiator to cross-link. This effect showed a strong dependence on the Rose Bengal concentration and it was concluded that the photopolymerization mechanism does not regenerate the dye. A few years later, the same group presented 2PP-induced collagen

cross-linking using the same photoinitiator to form stable sub-micron structures in fast processing timescales [69]. Since Rose Bengal displayed a low solubility at acidic pH, where collagens have the highest solubility, another photoinitiator that is soluble at acidic pH was developed. They reported a newly synthesized benzophenone dimer that could act as a photoinitiator for both BSA and collagen cross-linking [70]. Campagnola *et al.* also used Rose Bengal as the photoinitiator to process other proteins, such as fibrinogen, fibronectin, and concanavalin. Notably, the hydrogels prepared based on the above mentioned proteins maintained their bioactivity after the 2PP process [71].

Shear *et al.* used flavin adenine dinucleotide as a photoinitiator to fabricate interactive BSA or avidin-based microstructures in the presence of developing neurons [72]. They also created complex 3D architectures for neural cell guidance by crosslinking proteins within a HA hydrogel [57]. This group also used photocrosslinked proteins to create microstructures as compartments for cells and bacteria. By incorporating microscale density gradients of poly(methyl methacrylate) particles in crosslinked proteins, proteins with different hydration properties can be combined to achieve tunable volume changes that are rapid and reversible in response to changes in chemical environment [73].

3.2.2. Synthetic hydrogel precursors for two photon cross-linking

Synthetic hydrogels are appealing for tissue engineering because their chemical and physical properties are controllable and reproducible [45]. A 2PP-processable synthetic polymer used in tissue engineering must provide biocompatibility, biofunctionality, and appropriate mechanical properties. Biodegradability is also a requirement, if the cellular construct is designed to degrade after implantation [31]. To meet different application requirements, the material properties of the synthetic materials can be controlled by tuning molecular weights, block structures, degradable linkages, and crosslinking modes.

PEG is a key type of synthetic precursors and it has been widely used in tissue engineering. The mechanical properties and pore sizes of PEG based hydrogel constructs can be controlled over a wide range simply by tuning the molecular weight and/or the concentration of photopolymerizable PEG [74]. PEG based hydrogels facilitate the exploration of mechanical (elastic modulus, mesh size), geometrical (architecture), and chemical (cell adhesions peptides) effects on cell behavior and tissue growth [75].

West *et al.* took advantage of 2PP and its high resolution to cross-link PEGDA [76]. PEG derivatives were chosen because of their biocompatibility and resistance to protein adsorption and cell adhesion. Acrylate-terminated PEG macromers can be rapidly polymerized in the presence of the selected photoinitiator. This study demonstrated that the 3D structures fabricated from PEGDA hydrogels are capable of guiding and simultaneously restricting fibroblast cell migration. The same group also successfully fabricated 3D micropatterns of biomolecules in PEG hydrogels with collagenase-sensitive peptide chains, transforming a non-degradable and bioinert hydrogel into a degradable and cell-adhesive substrate [77].

Anseth *et al.* prepared PEG-based hydrogels to encapsulate human mesenchymal stem cells [78]. By introducing a nitrobenzyl ester-derived moiety into the PEG backbone, they demonstrated the ability to control hydrogel physical and chemical properties by incorporating various functional groups to control the degradation of the network. They also demonstrated that stem cell morphology could be controlled at any time through the degradation of the hydrogels using UV, visible or two photon irradiation [79]. Besides these topographical cues, the group was also able to immobilize thiol-containing biomolecules within a click-based hydrogel [78]. Upon gel formation, the hydrogel was soaked with fluorescently labelled, thiol-containing biomolecules together with a water soluble photoinitiator (eosin Y). Three dimensional biochemical structures were created at

high resolution (1 μm X/Y, 3-5 μm Z). The process was repeated to provide multiple adhesive signals relevant for many cell types. The group later synthesized biological molecules modified with thiol groups for photocoupling and photolabile moieties for photocleavage, which can be integrated to the PEG based hydrogel for additional functions [80]. These constructs provide a dynamic simplified synthetic environment with full spatiotemporal control and single factors can be varied selectively to achieve a better understanding of cell-microenvironment interactions existing in the native ECM [81].

3.2.3 Modified natural hydrogel precursors for two photon cross-linking

To achieve high reactivity and good biocompatibility of 2PP hydrogels precursors, researchers have developed chemically-modified natural polymers. For instance, methacrylated HA (HA-MA) has been explored as hydrogel precursor by Berg *et al*. [82] They prepared HA-MA through a reaction between primary hydroxyl groups of HA and methacrylic anhydride. The 2PP feasibility was proved with a very low writing speed (150 μm/s).

Ovsianikov *et al.* also performed studies on hydrogel cross-linking using modified naturally occurring macromolecules as monomers [83]. Methacrylamide-modified gelatin (GelMOD) and HA were used together with photoinitiator Irgacure 2959. Liska *et al.* also reported the synthesis of a vinyl ester derivative of gelatin (GH-VE) and its copolymerization with reduced BSA derivatives in the WSPI photoinitiator [83]. Well-defined scaffolds were fabricated with high 2PP writing speed (50 mm/ s) at low laser power (as low as 20 mW). The osteosarcoma cells were seeded inside the GH-VE/BSA scaffolds with various macromer ratios and GH-VE shows superior cytocompatibility. Loebel *et al.* demonstrated photo-crosslinking of tyramine-substituted hyaluronan (HA-Tyr) hydrogels for the first time [84]. HA-Tyr hydrogels are fabricated via a rapid

photosensitized process using visible light illumination. Nontoxic conditions offer photo-encapsulation of human mesenchymal stromal cells (hMSCs) with high viability. Macroscopic gels can be formed in less than 10 seconds. Different degrees of cross-linking induce different swelling/shrinking, allowing for light-induced microactuation. These new tools are complementary to the previously reported horseradish peroxidase/hydrogen peroxide cross-linking and allow sequential cross-linking of HA-Tyr matrices.

The photoinitiator and monomer are equally important in the 2PP process. Table 1 lists the reported photoinitiators with the corresponding hydrogels for 2PP fabrication.

Table 1 Photoinitiators with the corresponding hydrogels for 2PP fabrication

Photoinitiator				Hydrogel type	Cell type tested	Reference
Name	Water soluble	Commercial availability	σ_{2PA}			
Irgacure 369	No	Yes	7	PEGDA	Mouse fibroblasts	49
Irgacure 651/FA240	No	Yes	28	PEGDA/HEMA		52
Irgacure 819	No	Yes		PEGDA		85
Irgacure 2959	YES	Yes		GelMOD, HA	Human adipose-derived stem cells, porcine mesenchymal stem cells, fibroblasts, osteoblasts	53,83,86
LAP	Yes	Yes		PEGDA	10T1/2	54
Rose Bengal	Yes	Yes	10	BSA, fibrinogen, collagen, fibronectin,	Human dermal fibroblasts	68–70

				concanavalin A		
Benzophenone Dimer	Yes	Yes		BSA, collagen	human dermal fibroblasts	70
Flavin adenine dinucleotide (FAD)	Yes	Yes		BSA, avidin, PMMA	Cortical neurons, Escherichia coli	87
Methylene blue	Yes	Yes				
WSPI	Yes	No	120	PEGDA, gelatin derivative	C. elegans, osteosarcoma cells	88,89
G2CK	Yes	No	136	GelMOD	Human osteosarcoma cells	60,89
P2CK	Yes	No	76	GelMOD	Human osteosarcoma cells	60,89

Note:

σ_{2PA} : 2PA cross-sections in Göppert-Meyer (GM) units (10^{-50} cm^4 s $photon^{-1}$) ;

3.3 Resolution of 3D hydrogels fabricated by 2PP nanofabrication

The resolution is a key parameter for 3D hydrogels to precisely simulate the native 3D environment in which the cells reside. The improvement of the spatial resolution is very challenging, since 3D hydrogels can be easily deformed due to the high water content. The resolution of 3D hydrogels depends on the laser power and the exposure time of 2PP nanoprinting. The threshold energy of 2PP nanofabrication is also crucial for the resolution of 3D hydrogels. The resolution of 3D hydrogels can be improved by decreasing the threshold energy of 2PP 3D printing.

One convenient and direct method to improve the resolution of 2PP nano-printing is to use a highly

sensitive initiator. Duan *et al.* firstly used a facile assembly method to prepare a water soluble initiator by using a poloxamer (PF127) to encapsulate 2,7-bis(2-(4-pentaneoxy-phenyl)-vinyl)-anthraquinone via hydrophilic–hydrophobic assembly [90]. The polymerization threshold power was decreased to 6.29 mW and the lateral spatial resolution (LSR) was improved to 92 nm (Fig. 3). Moreover, 3D hydrogels simulating the morphology of adenovirus were prepared. In most of the previously published literatures, the finest resolution of 2PP is around 100 nm.

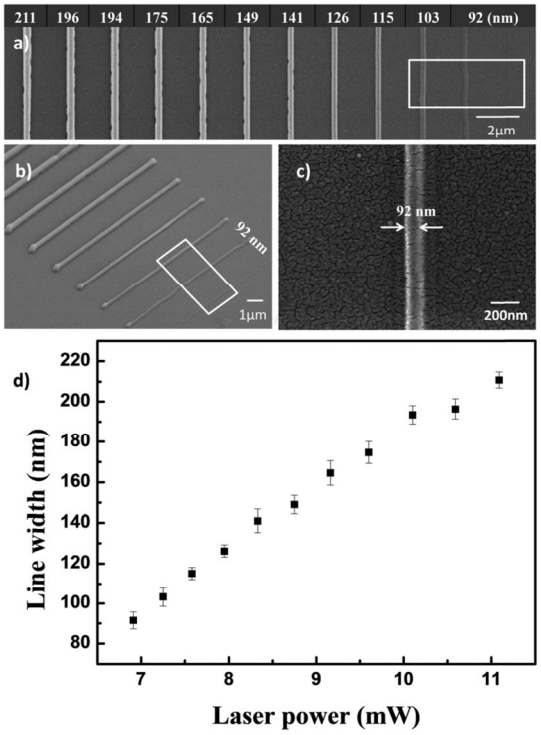

Fig. 3 (a) Top view and (b) side view of the SEM images of lines fabricated at a constant scanning speed of 10 mm/s with the laser power ranging from 11.09 to 6.29 mW. The selected areas shown in (a) and (b) represent the lines fabricated with laser power close to the laser threshold. (c) The magnified SEM image of the line of 92 nm. (d) The relationship of the laser power and the line width corresponding to (a). Reproduced from Ref. [90], Copyright Royal Society of Chemistry.

3.4 Applications on cellular tissue engineering

A considerable number of studies have been carried out on the complex cellular migratory response to the micro/nanostructures fabricated by 2PP. Such cellular responses depend on various factors such as the concentration of biomolecules, laser scanning speed and intensity, and other bioactive factors [91]. In the common practice of the cytotoxicity and proliferation tests, the cells are seeded on the fabricated scaffold or encapsulated in the hydrogel material. One important task in tissue engineering and regenerative medicine is to develop scaffolds with defined geometries. Such scaffolds should mimic the native environment of cells, enable the exchange of nutrients and metabolites, and serve as anchorage points for cell attachment in order to guide tissue formation in three dimensions. Such biocompatible scaffold materials have to be not only perfectly adaptable to the *in vivo* situation but also applicable for 3D structuring to provide well-defined, variable, reproducible, and stable scaffold geometry [92]. It is well-known that cell responses in a 3D environment can differ dramatically from *in vitro* 2D culturing conditions. Therefore, the fabrication of scaffolds with tailored geometry and porosity has great potential for investigating cell behavior in 3D.

The natural cellular environment features complex 3D structures at multiple length scales. Many *in vitro* studies of cell behavior in 3D rely on the availability of artificial scaffolds with controlled 3D topologies. Ovsianikov *et al.* demonstrated the fabrication of 3D scaffolds for tissue engineering out of PEGDA materials by means of 2PP (Fig. 4(a)) [50]. The spatial resolution dependence on the applied irradiation parameters was investigated for two PEGDA formulations with molecular weights of 302 and 742. Minimum feature sizes of 200 nm were achieved in both materials. They also studied the cytotoxicity of the material formulations with respect to photoinitiator type and photoinitiator concentration. Aqueous extracts from photopolymerized

PEGDA samples indicated the presence of water-soluble molecules that are toxic to fibroblasts. It was shown that sample aging in aqueous medium reduced the cytotoxicity of these extracts and this mechanism provides a route for biomedical applications of structures fabricated by 2PP technologies in general. The results suggest that 2PP may be used to polymerize PEG-based materials into 3D scaffolds that mimic the physical and biological properties of native cell environments.

Although commercially available PEGDA has been widely used to fabricate a 3D hydrogel due to its high reactivity and tunable physical properties, the interaction between cells and PEGDA is known to be rather weak and new hydrophilic monomers/oligomers are required to improve the bioactivity of the formed scaffolds. Monomers/oligomers derived from natural polymers, especially from those that are components of the native ECM should be considered. Hyaluronic acid (HA) is a major component of human ECM and it represents an extremely attractive starting material for the fabrication of scaffolds for tissue engineering. Due to the poor mechanical strength of HA hydrogels, structural fabrication of this material class remains a major challenge. Kufelt *et al.* combined HA with PEGDA to prepare 3D hydrogel scaffolds with different compositions in order to examine the biological and mechanical properties of the photo-crosslinked materials (Fig. 4(b)) [86]. Cell testing with osteoblasts confirmed the compatibility of the materials for the future usage as biomatrices for guided bone formation. In addition, different ratios of PEGDA vs. HA were used to modulate the mechanical properties of the generated gels without affecting the biocompatibility. With 2PP, precisely defined 3D HA and HA–PEGDA scaffolds with different geometries and pore sizes were successfully fabricated. Such structures provided promising prospects for cell investigations in a reproducible 3D organized hydrogel milieu.

Ovsianikov *et al.* also carried out studies on hydrogel cross-linking using modified naturally

occurring macromolecules as monomers. They used modified gelatin-GelMOD and HA together with Irgacure 2959 initiator to develop precisely defined biodegradable 3D tissue engineering scaffolds (Fig. 4(c)) [83]. The fabricated scaffolds provided good conditions for the attachment of porcine mesenchymal stem cells and their subsequent proliferation. Upon applying an osteoinductive medium, the cells showed calcium deposition on the 3D scaffold. The results show that hydrogel structures engineered accurately via CAD and 2PP can lead to novel perspectives for studying tissue formation in 3D.

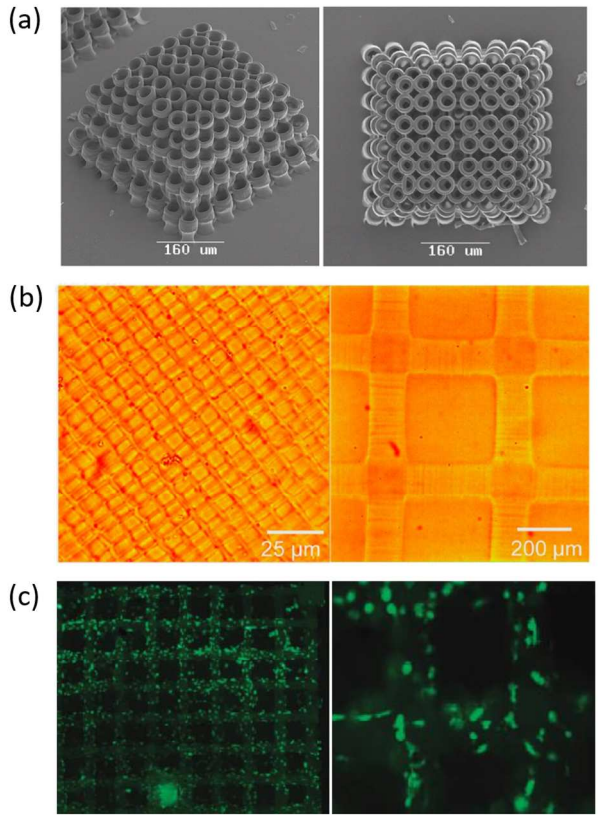

Fig. 4 (a) Scanning electron microscope images of 2PP fabricated scaffold for tissue engineering. (b) Optical microscopic images of grid-like scaffolds with different grid sizes. (c) Fluorescent images of scaffold and seeded cells. Adapted from Ref. [50], copyright 2010 Acta Materialia Inc.; from Ref. [86], copyright 2014 American Chemical Society; and from Ref. [83], copyright 2011 American Chemical Society.

Natural tissues and their cellular microenvironment have complex structural and biological heterogeneity and are constantly exposed to a myriad of forces. Structure–function relationships of cell–material interactions have been investigated using various approaches. Cells generate contractile forces on their underlying substrate. Alterations in elastic modulus impact a variety of cell types in fundamentally different ways including motility, gene expression, proliferation, and fate after differentiation. Although elastic modulus has been intensively studied in cell–material interaction researches, another aspect of the material's mechanical properties, namely the Poisson's ratio, is rarely investigated due to the technical difficulty in fabricating biomaterials with tunable Poisson's ratio.

2PP 3D printing has been used to fabricate suspended web structures that exhibit positive and negative Poisson's ratios (PPR and NPR) based on analytical models (Fig. 5). [54,93,94] NPR webs demonstrate biaxial expansion/compression behavior as one or multiple cells apply local forces and move the structures. To evaluate cell response, 10T1/2 cells were seeded on the web structures and cell movement was captured using time-lapse microscopy. The observations suggest that unusual cell division can be induced solely by the NPR structure in the absence of any external biochemical manipulations to the cell components.

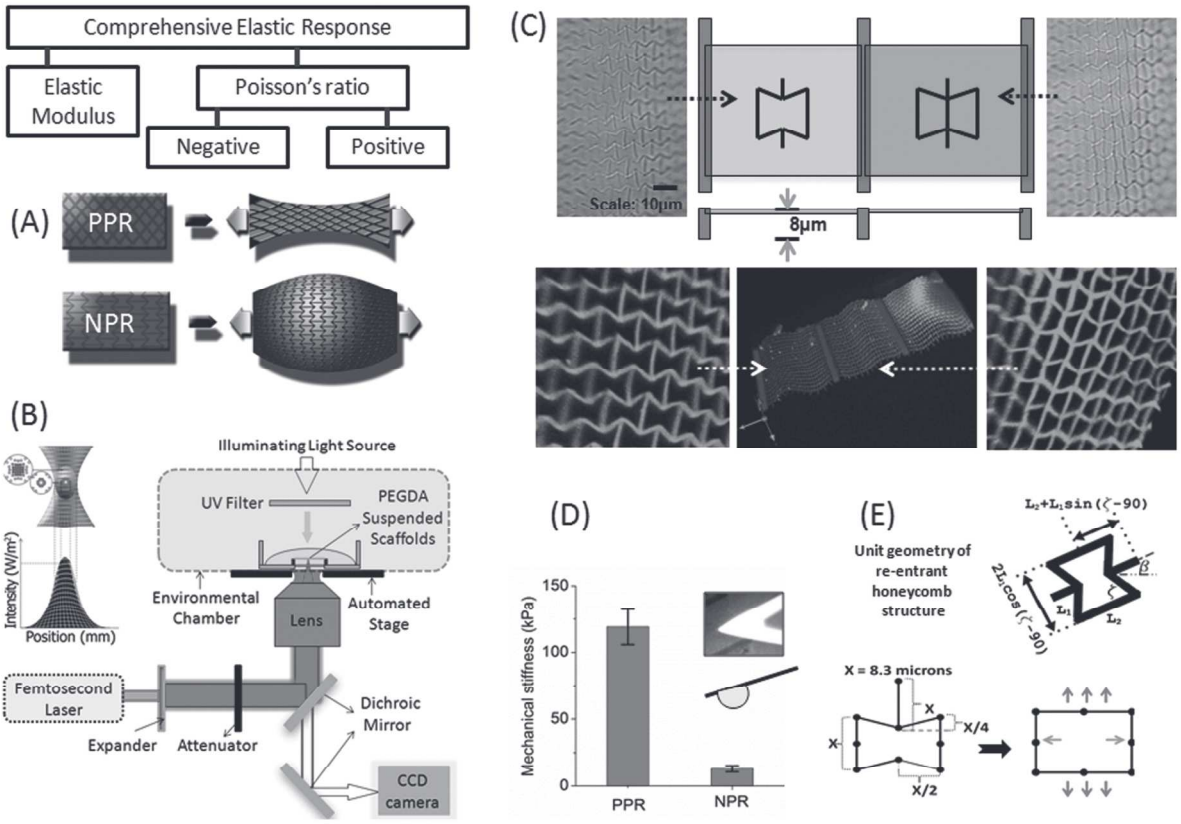

Figure 5. A) The elastic property of a biomaterial can be comprehensively expressed by the elastic modulus and the Poisson's ratio. Schematic shows a PPR material contracting transversally when axially stretched, while a NPR material expanding in both the axial and transverse directions. B) Schematic of the two-photon absorption process and the femtosecond laser fabrication set-up. C) Optical and confocal images of NPR and PPR suspended web structures with side supports using PEGDA biomaterial. D) AFM measurements using a 20 μm bead measures the effective stiffness of NPR and PPR web structures in the z -direction. E) Re-entrant honeycomb configuration was adopted as the unit cell geometry for the NPR web, while an additional strut modification to the NPR structure served as the positive control. Schematic shows biaxial expansion of the NPR structure upon axial strains (arrows). Reproduced from Ref [54], copyright 2013 WILEY-VCH Verlag GmbH & Co. KGaA, Weinheim.

4. Conclusions and future perspectives

2PP has been demonstrated as a promising tool for creating micro and nano-devices based on hydrogel biomaterials. These hydrogel devices have been used as: (a) barriers following tissue injury to ensure better healing, (b) localized drug delivery systems, (c) cell cages in order to ensure

cell transplantation, and (d) scaffold materials for regeneration of soft tissues [95].

A critical issue of 2PP is the processing time. Using point by point scanning processing, fabricating millimeter sized constructs might take a few hours or even days. With microlens arrays or diffractive optical elements (DOEs), a femtosecond laser beam can be split into tens or even hundreds of spots [96] thus increasing the throughput. However, this technology is only suitable for the fabrication of periodic structures. To improve the throughput of femtosecond laser fabrication, Li *et al.* modulated the femtosecond laser beam using a spatial light modulator (SLM) to realize the parallel processing [97] and shot exposure processing [98,99]. This will greatly improve the 2PP processing efficiency.

Due to the limitations of the optical, mechanical and chemical properties of the hydrogel, it is still challenging to fabricate microstructures in hydrogels with precise control over shape and pore dimensions at the sub-100 nm scale. Inspired by stimulated emission depletion microscopy [100], super-resolution laser direct writing technique has been invented, which pushed the fabrication resolution to around 60 nm [101–104]. Further work needs to be focused on the design and preparation of highly efficient 2PP initiators and appropriate photopolymerizable monomers/macromers. More importantly, rapid processing methods should be developed to meet the high throughput demand for the industrial mass production of hydrogel scaffolds.

Conflict of Interest

There are no conflicts to declare.

Acknowledgement

The work was supported in part by grants from the California Institute for Regenerative Medicine (RT3-07899), National Institutes of Health (R01EB021857, R21HD090662) and National Science Foundation (CMMI 1547005, CMMI-1644967)

Reference

1 N. Annabi, J. W. Nichol, X. Zhong, C. Ji, S. Koshy, A. Khademhosseini and F. Dehghani, *Tissue Eng. Part B Rev.*, 2010, **16**, 371–383.

2 N. Annabi, A. Tamayol, J. A. Uquillas, M. Akbari, L. E. Bertassoni, C. Cha, G. Camci-Unal, M. R. Dokmeci, N. A. Peppas and A. Khademhosseini, *Adv. Mater.*, 2014, **26**, 85–124.

3 M. E. Gomes, M. T. Rodrigues, R. M. A. Domingues and R. L. Reis, *Tissue Eng. Part B Rev.*, 2017, **23**, 211–224.

4 P. Soman, B. T. D. Tobe, J. W. Lee, A. A. M. Winquist, I. Singec, K. S. Vecchio, E. Y. Snyder and S. Chen, *Biomed. Microdevices*, 2012, **14**, 829–838.

5 C. Cha, P. Soman, W. Zhu, M. Nikkhah, G. Camci-Unal, S. Chen and A. Khademhosseini, *Biomater Sci*, 2014, **2**, 703–709.

6 F. Zheng, F. Fu, Y. Cheng, C. Wang, Y. Zhao and Z. Gu, *Small*, 2016, **12**, 2253–2282.

7 A. Vashist, A. Vashist, Y. K. Gupta and S. Ahmad, *J Mater Chem B*, 2014, **2**, 147–166.

8 J. Tavakoli and Y. Tang, *Polymers*, 2017, **9**, 364.

9 L. Li, Y. Shi, L. Pan, Y. Shi and G. Yu, *J. Mater. Chem. B*, 2015, **3**, 2920–2930.

10 M. Li, Q. Yang, H. Liu, M. Qiu, T. J. Lu and F. Xu, *Small*, 2016, **12**, 4492–4500.

11 O. Veiseh, J. C. Doloff, M. Ma, A. J. Vegas, H. H. Tam, A. R. Bader, J. Li, E. Langan, J. Wyckoff and W. S. Loo, *Nat. Mater.*, 2015, **14**, 643–651.

12 I. A. Eydelnant, B. B. Li and A. R. Wheeler, *Nat. Commun.*, 2014, **5**, 3355.

13 Y. L. Han, Y. Yang, S. Liu, J. Wu, Y. Chen, T. J. Lu and F. Xu, *Biofabrication*, 2013, **5**, 035004.

14 F. Xu, C. M. Wu, V. Rengarajan, T. D. Finley, H. O. Keles, Y. Sung, B. Li, U. A. Gurkan and U. Demirci, *Adv. Mater.*, 2011, **23**, 4254–4260.

15 S. Muro, C. Garnacho, J. A. Champion, J. Leferovich, C. Gajewski, E. H. Schuchman, S. Mitragotri and V. R. Muzykantov, *Mol. Ther.*, 2008, **16**, 1450–1458.

16 W. Bian, B. Liau, N. Badie and N. Bursac, *Nat. Protoc.*, 2009, **4**, 1522–1534.

17 K. R. Stevens, M. D. Ungrin, R. E. Schwartz, S. Ng, B. Carvalho, K. S. Christine, R. R. Chaturvedi, C. Y. Li, P. W. Zandstra and C. S. Chen, *Nat. Commun.*, 2013, **4**, 1847.

18 D. Qin, Y. Xia and G. M. Whitesides, *Nat. Protoc.*, 2010, **5**, 491–502.

19 S. Hong, D. Sycks, H. F. Chan, S. Lin, G. P. Lopez, F. Guilak, K. W. Leong and X.

Zhao, *Adv. Mater.*, 2015, **27**, 4035–4040.

20 W. Zhu, X. Ma, M. Gou, D. Mei, K. Zhang and S. Chen, *Curr. Opin. Biotechnol.*, 2016, **40**, 103–112.

21 F. Yanagawa, S. Sugiura and T. Kanamori, *Regen. Ther.*, 2016, **3**, 45–57.

22 R. Guo, S. Xiao, X. Zhai, J. Li, A. Xia and W. Huang, *Opt. Express*, 2006, **14**, 810–816.

23 S.-H. Park, D.-Y. Yang and K.-S. Lee, *Laser Photonics Rev.*, 2009, **3**, 1–11.

24 L. Amato, Y. Gu, N. Bellini, S. M. Eaton, G. Cerullo and R. Osellame, *Lab. Chip*, 2012, **12**, 1135–1142.

25 J. Torgersen, X.-H. Qin, Z. Li, A. Ovsianikov, R. Liska and J. Stampfl, *Adv. Funct. Mater.*, 2013, **23**, 4542–4554.

26 F. Claeyssens, E. A. Hasan, A. Gaidukeviciute, D. S. Achilleos, A. Ranella, C. Reinhardt, A. Ovsianikov, X. Shizhou, C. Fotakis and M. Vamvakaki, *Langmuir*, 2009, **25**, 3219–3223.

27 A. Selimis, V. Mironov and M. Farsari, *Microelectron. Eng.*, 2015, **132**, 83–89.

28 S. Maruo, O. Nakamura and S. Kawata, *Opt. Lett.*, 1997, **22**, 132–134.

29 W. R. Zipfel, R. M. Williams and W. W. Webb, *Nat. Biotechnol.*, 2003, **21**, 1369–1377.

30 S. Wu, J. Serbin and M. Gu, *J. Photochem. Photobiol. Chem.*, 2006, **181**, 1–11.

31 M. T. Raimondi, S. M. Eaton, M. M. Nava, M. Laganà, G. Cerullo and R. Osellame, *J Appl Biomater Biomech*, 2012, **10**, 55–65.

32 A. Ovsianikov, *Investigation of two-photon polymerization technique for applications in photonics and biomedicine*, Cuvillier, 2009.

33 H.-B. Sun and S. Kawata, *Adv. Polym. Sci.*, 2004, **170**, 169–274.

34 K. Obata, A. El-Tamer, L. Koch, U. Hinze and B. N. Chichkov, *Light Sci. Appl.*, 2013, **2**, e116–e116.

35 S. Maruo and J. T. Fourkas, *Laser Photonics Rev.*, 2008, **2**, 100–111.

36 C. N. LaFratta, J. T. Fourkas, T. Baldacchini and R. A. Farrer, *Angew. Chem. Int. Ed.*, 2007, **46**, 6238–6258.

37 K. J. Schafer, J. M. Hales, M. Balu, K. D. Belfield, E. W. Van Stryland and D. J. Hagan, *J. Photochem. Photobiol. Chem.*, 2004, **162**, 497–502.

38 Z. Li, N. Pucher, K. Cicha, J. Torgersen, S. C. Ligon, A. Ajami, W. Husinsky, A. Rosspeintner, E. Vauthey, S. Naumov, T. Scherzer, J. Stampfl and R. Liska, *Macromolecules*, 2013, **46**, 352–361.

39 M. Chen, M. Zhong and J. A. Johnson, *Chem. Rev.*, 2016, **116**, 10167–10211.

40 S. Juodkazis, V. Mizeikis and H. Misawa, *J. Appl. Phys.*, 2009, **106**, 051101.

41 W.-E. Lu, X.-Z. Dong, W.-Q. Chen, Z.-S. Zhao and X.-M. Duan, *J. Mater. Chem.*, 2011, **21**, 5650–5659.

42 Y. Li, L. Chen, F. Kong, Z. Wang, M. Dao, C. T. Lim, F. Li and M. Hong, *Opto-Electron. Eng.*, 2017, **44**, 393–399.

43 K. Kim, W. Zhu, X. Qu, C. Aaronson, W. R. McCall, S. Chen and D. J. Sirbuly, *ACS Nano*, 2014, **8**, 9799–9806.

44 D. L. Alge and K. S. Anseth, *Nat. Mater.*, 2013, **12**, 950–952.

45 J. L. Drury and D. J. Mooney, *Biomaterials*, 2003, **24**, 4337–4351.

46 J.-F. Xing, M.-L. Zheng and X.-M. Duan, *Chem. Soc. Rev.*, 2015, **44**, 5031–5039.

47 K. Cicha, Z. Li, K. Stadlmann, A. Ovsianikov, R. Markut-Kohl, R. Liska and J. Stampfl, *J. Appl. Phys.*, 2011, **110**, 064911.

48 A. Ovsianikov, S. Schlie, A. Ngezahayo, A. Haverich and B. N. Chichkov, *J. Tissue Eng. Regen. Med.*, 2007, **1**, 443–449.

49 A. Ovsianikov, M. Gruene, M. Pflaum, L. Koch, F. Maiorana, M. Wilhelmi, A. Haverich and B. Chichkov, *Biofabrication*, 2010, **2**, 014104.

50 A. Ovsianikov, M. Malinauskas, S. Schlie, B. Chichkov, S. Gittard, R. Narayan, M. Löbler, K. Sternberg, K.-P. Schmitz and A. Haverich, *Acta Biomater.*, 2011, **7**, 967–974.

51 T. Wei\s s, R. Schade, T. Laube, A. Berg, G. Hildebrand, R. Wyrwa, M. Schnabelrauch and K. Liefeith, *Adv. Eng. Mater.*, 2011, **13**, B264–B273.

52 S. J. Jhaveri, J. D. McMullen, R. Sijbesma, L.-S. Tan, W. Zipfel and C. K. Ober, *Chem. Mater.*, 2009, **21**, 2003–2006.

53 A. Ovsianikov, A. Deiwick, S. Van Vlierberghe, M. Pflaum, M. Wilhelmi, P. Dubruel and B. Chichkov, *Materials*, 2011, **4**, 288–299.

54 W. Zhang, P. Soman, K. Meggs, X. Qu and S. Chen, *Adv. Funct. Mater.*, 2013, **23**, 3226–3232.

55 M. Farsari, G. Filippidis, K. Sambani, T. S. Drakakis and C. Fotakis, *J. Photochem. Photobiol. -Chem.*, 2006, **181**, 132–135.

56 S. Basu, V. Rodionov, M. Terasaki and P. J. Campagnola, *Opt. Lett.*, 2005, **30**, 159–161.

57 S. K. Seidlits, C. E. Schmidt and J. B. Shear, *Adv. Funct. Mater.*, 2009, **19**, 3543–3551.

58 E. C. Spivey, E. T. Ritschdorff, J. L. Connell, C. A. McLennon, C. E. Schmidt and J.

B. Shear, *Adv. Funct. Mater.*, 2013, **23**, 333–339.

59 J. Torgersen, A. Ovsianikov, V. Mironov, N. Pucher, X. Qin, Z. Li, K. Cicha, T. Machacek, R. Liska and V. Jantsch, *J. Biomed. Opt.*, 2012, **17**, 105008–105008.

60 A. Ovsianikov, S. Mühleder, J. Torgersen, Z. Li, X.-H. Qin, S. Van Vlierberghe, P. Dubruel, W. Holnthoner, H. Redl and R. Liska, *Langmuir*, 2013, **30**, 3787–3794.

61 J. Xing, J. Liu, T. Zhang, L. Zhang, M. Zheng and X. Duan, *J. Mater. Chem. B*, 2014, **2**, 4318–4323.

62 D. Bhatnagar, M. Simon and M. H. Rafailovich, in *Recent Advances in Biopolymers*, ed. F. K. Parveen, InTech, 2016.

63 J. A. Hunt, R. Chen, T. van Veen and N. Bryan, *J Mater Chem B*, 2014, **2**, 5319–5338.

64 S. J. Buwalda, K. W. M. Boere, P. J. Dijkstra, J. Feijen, T. Vermonden and W. E. Hennink, *J. Controlled Release*, 2014, **190**, 254–273.

65 D. B. Berry, S. You, J. Warner, L. R. Frank, S. Chen and S. R. Ward, *Tissue Eng. Part A*, , DOI:10.1089/ten.tea.2016.0438.

66 W. Zhu, X. Qu, J. Zhu, X. Ma, S. Patel, J. Liu, P. Wang, C. S. E. Lai, M. Gou, Y. Xu, K. Zhang and S. Chen, *Biomaterials*, 2017, **124**, 106–115.

67 X. Ma, X. Qu, W. Zhu, Y.-S. Li, S. Yuan, H. Zhang, J. Liu, P. Wang, C. S. E. Lai and F. Zanella, *Proc. Natl. Acad. Sci.*, 2016, **113**, 2206–2211.

68 J. D. Pitts, P. J. Campagnola, G. A. Epling and S. L. Goodman, *Macromolecules*, 2000, **33**, 1514–1523.

69 L. P. Cunningham, M. P. Veilleux and P. J. Campagnola, *Opt. Express*, 2006, **14**, 8613–8621.

70 S. Basu, L. P. Cunningham, G. D. Pins, K. A. Bush, R. Taboada, A. R. Howell, J. Wang and P. J. Campagnola, *Biomacromolecules*, 2005, **6**, 1465–1474.

71 S. Basu and P. J. Campagnola, *J. Biomed. Mater. Res. A*, 2004, **71**, 359–368.

72 B. Kaehr, R. Allen, D. J. Javier, J. Currie and J. B. Shear, *Proc. Natl. Acad. Sci. U. S. A.*, 2004, **101**, 16104–16108.

73 B. Kaehr and J. B. Shear, *Proc. Natl. Acad. Sci.*, 2008, **105**, 8850–8854.

74 Q. T. Nguyen, Y. Hwang, A. C. Chen, S. Varghese and R. L. Sah, *Biomaterials*, 2012, **33**, 6682–6690.

75 H. Liao, D. Munoz-Pinto, X. Qu, Y. Hou, M. A. Grunlan and M. S. Hahn, *Acta Biomater.*, 2008, **4**, 1161–1171.

76 M. S. Hahn, J. S. Miller and J. L. West, *Adv. Mater.*, 2006, **18**, 2679–2684.

77 S.-H. Lee, J. J. Moon and J. L. West, *Biomaterials*, 2008, **29**, 2962–2968.

78 C. A. DeForest and K. S. Anseth, *Nat. Chem.*, 2011, **3**, 925–931.

79 A. M. Kloxin, A. M. Kasko, C. N. Salinas and K. S. Anseth, *Science*, 2009, **324**, 59–63.

80 C. A. DeForest and K. S. Anseth, *Angew. Chem.*, 2012, **124**, 1852–1855.

81 A. I. Ciuciu and P. J. Cywiński, *RSC Adv.*, 2014, **4**, 45504–45516.

82 A. Berg, R. Wyrwa, J. Weisser, T. Weiss, R. Schade, G. Hildebrand, K. Liefeith, B. Schneider, R. Ellinger and M. Schnabelrauch, *Adv. Eng. Mater.*, 2011, **13**, B274–B284.

83 A. Ovsianikov, A. Deiwick, S. Van Vlierberghe, P. Dubruel, L. Möller, G. Dräger and B. Chichkov, *Biomacromolecules*, 2011, **12**, 851–858.

84 C. Loebel, N. Broguiere, M. Alini, M. Zenobi-Wong and D. Eglin, *Biomacromolecules*, 2015, **16**, 2624–2630.

85 W. Zhang and S. Chen, *MRS Bull.*, 2011, **36**, 1028–1033.

86 O. Kufelt, A. El-Tamer, C. Sehring, S. Schlie-Wolter and B. N. Chichkov, *Biomacromolecules*, 2014, **15**, 650–659.

87 H. Y. Woo, B. Liu, B. Kohler, D. Korystov, A. Mikhailovsky and G. C. Bazan, *J. Am. Chem. Soc.*, 2005, **127**, 14721–14729.

88 X.-H. Qin, J. Torgersen, R. Saf, S. Mühleder, N. Pucher, S. C. Ligon, W. Holnthoner, H. Redl, A. Ovsianikov and J. Stampfl, *J. Polym. Sci. Part Polym. Chem.*, 2013, **51**, 4799–4810.

89 Z. Li, J. Torgersen, A. Ajami, S. Mühleder, X. Qin, W. Husinsky, W. Holnthoner, A. Ovsianikov, J. Stampfl and R. Liska, *RSC Adv.*, 2013, **3**, 15939–15946.

90 J. Xing, L. Liu, X. Song, Y. Zhao, L. Zhang, X. Dong, F. Jin, M. Zheng and X. Duan, *J. Mater. Chem. B*, 2015, **3**, 8486–8491.

91 M.-L. Zheng, J.-F. Xing and X.-M. Duan, in *Smart Materials for Tissue Engineering*, 2016, pp. 441–468.

92 B. V. Slaughter, S. S. Khurshid, O. Z. Fisher, A. Khademhosseini and N. A. Peppas, *Adv. Mater.*, 2009, **21**, 3307–3329.

93 P. Soman, D. Y. Fozdar, J. W. Lee, A. Phadke, S. Varghese and S. Chen, *Soft Matter*, 2012, **8**, 4946.

94 P. Soman, J. W. Lee, A. Phadke, S. Varghese and S. Chen, *Acta Biomater.*, 2012, **8**, 2587–2594.

95 K. T. Nguyen and J. L. West, *Biomaterials*, 2002, **23**, 4307–4314.

96 S. You, C. Kuang, K. C. Toussaint, R. Zhou, X. Xia and X. Liu, *Opt. Lett.*, 2015, **40**, 3532.

97 L. Yang, A. El-Tamer, U. Hinze, J. Li, Y. Hu, W. Huang, J. Chu and B. N. Chichkov, *Opt. Lasers Eng.*, 2015, **70**, 26–32.

98 L. Yang, A. El-Tamer, U. Hinze, J. Li, Y. Hu, W. Huang, J. Chu and B. N. Chichkov, *Appl. Phys. Lett.*, 2014, **105**, 041110.

99 C. Zhang, Y. Hu, J. Li, Z. Lao, J. Ni, J. Chu, W. Huang and D. Wu, *Appl. Phys. Lett.*, 2014, **105**, 221104.

100 S. W. Hell and J. Wichmann, *Opt. Lett.*, 1994, **19**, 780.

101 J. Fischer and M. Wegener, *Laser Photonics Rev.*, 2013, **7**, 22–44.

102 L. Li, R. R. Gattass, E. Gershgoren, H. Hwang and J. T. Fourkas, *Science*, 2009, **324**, 910–913.

103 T. F. Scott, B. A. Kowalski, A. C. Sullivan, C. N. Bowman and R. R. McLeod, *Science*, 2009, **324**, 913–917.

104 T. L. Andrew, H.-Y. Tsai and R. Menon, *Science*, 2009, **324**, 917–921.

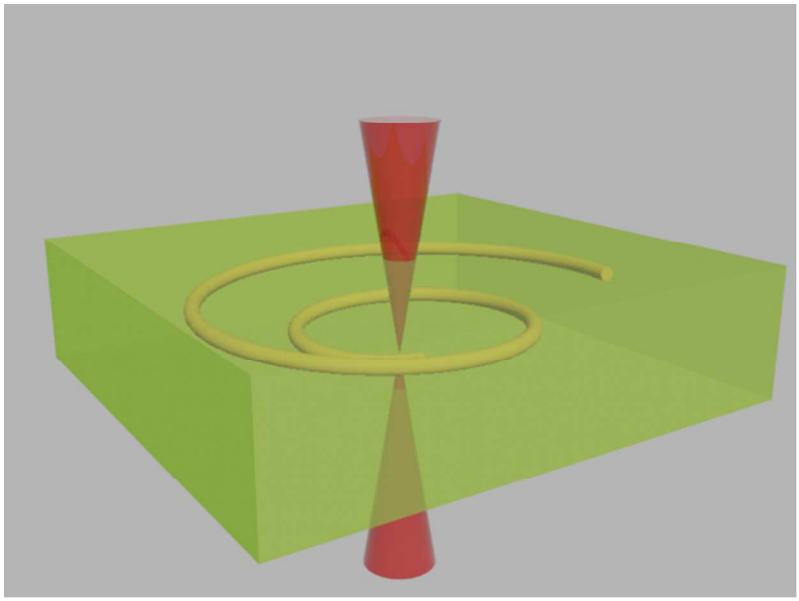

Two-photon polymerization enables nanoscale 3D printing of hydrogels.